A simple model for examining issues in radiotherapy optimization

David M. Shepard,[a] Gustavo Olivera, Lisa Angelos, Otto Sauer, Paul Reckwerdt, and T. Rockwell Mackie
Department of Medical Physics, University of Wisconsin–Madison, Madison, Wisconsin 53706-1532

(Received 18 May 1998; accepted for publication 30 March 1999)

Convolution/superposition software has been used to produce a library of photon pencil beam dose matrices. This library of pencil beams is designed to serve as a tool for both education and investigation in the field of radiotherapy optimization. The elegance of this pencil beam model stems from its cylindrical symmetry. Because of the symmetry, the dose distribution for a pencil beam from any arbitrary angle can be determined through a simple rotation of a pre-computed dose matrix. Rapid dose calculations can thus be performed while maintaining the accuracy of a convolution/superposition based dose computation. The pencil beam data sets have been made publicly available. It is hoped that the data sets will facilitate a comparison of a variety of optimization and delivery approaches. This paper will present a number of studies designed to demonstrate the usefulness of the pencil beam data sets. These studies include an examination of the extent to which a treatment plan can be improved through either an increase in the number of beam angles and/or a decrease in the collimator size. A few insights into the significance of heterogeneity corrections for treatment planning for intensity modulated radiotherapy will also be presented.
 [S0094-2405(99)02007-6]

I. INTRODUCTION

In recent years, the development of intensity modulated radiation therapy (IMRT) has provided many new opportunities in the delivery of conformal radiotherapy.[1–13] There are, however, many unanswered questions about this new method of treatment delivery. The goal of this project has been the development of a test environment that provides a means for efficiently investigating some of the unresolved issues in IMRT. The test environment is also designed to serve as an educational tool that can benefit those who wish to learn more about this emerging field.

In research fields ranging from cellular biology to economics, investigators have often used models to improve their understanding of complex problems. With a model that is well designed, one can analyze a difficult problem in a more manageable form. Despite the incorporation of numerous simplifying assumptions, a model can provide investigators with key insights while minimizing time demands.

This paper will present a radiotherapy model that is intended to serve as a tool in studying IMRT. Because this model includes a number of simplifying assumptions, it cannot be used to provide specific conclusions regarding individual disease sites. Rather, it is designed to enhance our understanding of optimization algorithms and proposed delivery techniques.

This project involved the computation of three pencil beam data sets. The data sets and the convolution code used to produce them are available through our web site at www.madrad.radiology.wisc.edu. It is hoped that these pencil beams will provide a means of comparing proposed optimization and delivery techniques. The goal of this paper is to provide a description of the data sets and to demonstrate the usefulness of these data in a variety of optimization studies.

II. MATERIALS AND METHODS

A. Dose computation

A convolution/superposition method[14–16] was used to determine the dose delivered to a cylindrical phantom by a series of photon pencil beams.[17] The computations were performed for three distinct phantom setups. The first simulated phantom was a 20-cm-diameter all-water cylinder with a density of 1 g/cm^3 [see Fig. 1(a)].

The second simulated phantom used two cylinders sharing a common central axis. The inner cylinder had a 10 cm diameter, and the outer cylinder had a 20 cm diameter. The material located within the inner cylinder was assigned a density of 0.3 g/cm^3 (''lung''), and the region between the two cylinders was assigned a density of 1.0 g/cm^3 (''water''). Circular symmetry was maintained with this setup. This phantom was primarily designed to evaluate the importance of heterogeneity corrections in IMRT treatment planning.

For both setups, the outer cylinder was surrounded by a medium of density zero, and the cylinders were partitioned into voxels 0.2 cm on each side. With these setups, we did not model either the geometric penumbra or the collimator transmission. Intensity horns were not included, but they can easily be accounted for in the optimization. With small pencil beam sizes, not including the horns will have very little effect on the final dose distribution. This is because the horns can be accounted for by modifying the final beam weights before determining the actual intensity pattern that needs to be delivered.

In Fig. 1(a), pencil beam one illustrates the geometry for a single pencil beam entering from the top of the phantom. The geometry of the delivery was such that each pencil beam

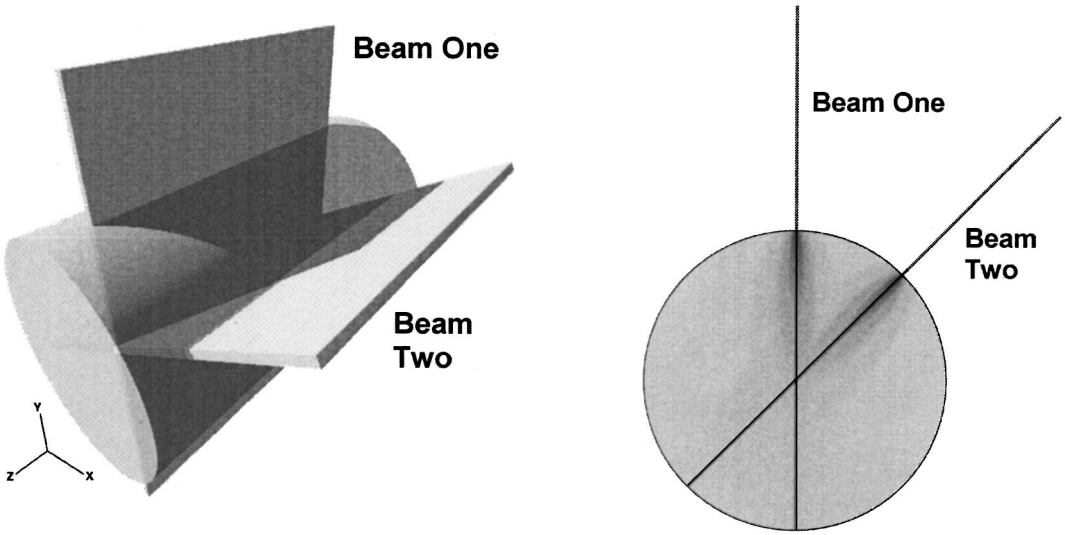

FIG. 1. (a) The geometry of the first phantom and the corresponding beam delivery. Pencil beam one is a parallel pencil beam. Because of the symmetry of the setup, the dose distribution for pencil beam two can be determined by simply rotating pencil beam one through 45 degrees. (b) The geometry in the central slice of the phantom.

covered a 10 cm length of the cylinder along the z-axis. The field size of each beam in the x-direction was set to 0.2 cm. Each beam was a 2-MeV monoenergetic photon pencil beam with parallel rays and each had a uniform intensity over its cross-section. For each beam, the voxel receiving the highest dose was normalized to an energy fluence of one. The elongated extent (10 cm) of the pencil beams was such that we could take into account lateral contributions of electrons and scattered photons to the central axis plan from a reasonably sized beam.

Figure 2(a) shows an isodose plot from a pencil beam entering from the top of the phantom. For a single beam direction, one pencil beam was computed per point of incidence on the cylindrical phantom. Thus from this single direction, 99 photon pencil beams were computed.

Due to the symmetric nature of both the phantom and the irradiation, one can obtain the dose from any arbitrary angle through a simple rotation of a pre-computed dose matrix. The dose matrix is rotated around the central axis of the cylinder. Pencil beam two in Figs. 1(a) and 1(b) was obtained by a 45-degree rotation of pencil beam one. An isodose plot of this beam is shown in Fig. 2(b). The model thus maintains the accuracy of a convolution based dose computation without the need for further time consuming convolution/superposition calculations.

A third phantom setup made use of a 33-cm-diameter cylinder with the isocenter placed at 93 cm. The beams were diverging, and each beam projected to a width of 3 mm and a height of 7.6 mm at isocenter. A polyenergetic spectrum was used with a maximum energy of 4 MeV and a mean energy of 1.4 MeV. A source size of 1.5 mm was used. These specifications were chosen to match the beam characteristics of our tomotherapy workbench.

The convolution/superposition method was chosen for the dose computations because of its ability to accurately model the dose distribution. The computation began with a determination of the distribution of TERMA (total energy released per unit mass) in the phantom due to photons generated in the accelerator. This TERMA distribution was then convolved with a kernel derived from Monte Carlo simulation. The kernel accounted for the transport of charged particles as well as scattered photons generated in the phantom.[16]

Electron contamination was neglected in these dose computations. Therefore, any conclusions that are derived using these beams might not apply to targets located in regions close to the surface of the phantom.

After computing the three-dimensional dose matrices, the dose to the central slice of the phantom was extracted. For each pencil beam, the dose to the central slice can be represented with a two-dimensional matrix. Figure 1(b) shows the geometry for pencil beam one in the central slice.

B. Treatment plan optimization

MATLAB (The Mathworks Inc., Natick, MA) has served as a useful tool for processing the pencil beam data sets. MATLAB is a numeric computation and visualization software system that incorporates a general purpose optimization package.

The development of each treatment plan follows four basic steps:

(1) The pencil beam dose matrices are loaded into MATLAB.
(2) The locations of both targets and regions at risk are specified.

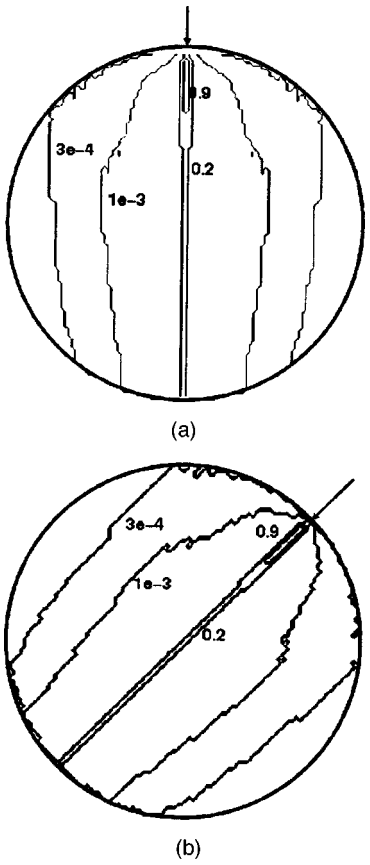

FIG. 2. (a) An isodose plot of an individual pencil beam in the central slice of the phantom. (b) The same beam rotated through 45 degrees. The dose does not need to be recomputed as a result of the symmetry.

(3) The beams are rotated to the desired angles.
(4) The beam intensity distributions are optimized to develop the most favorable dose distribution.

For the studies presented in this paper, equispaced beam angles were used. The results for the few field optimizations could potentially be improved with the use of optimally selected beam angles.[18] Unfortunately, the problem of determining the optimal angles for intensity-modulated beam delivery is one of the most difficult in radiotherapy.[3]

Each simulation uses a target placed within the central slice. The voxels of the target are assumed to have the same density as the phantom. Thus the target does not alter the pre-computed dose matrices. Along with the target, one or more regions at risk (RARs) are placed in the circular slice.

A number of target shapes have been tested. In order to test a simple target, a square shaped target was used with a smaller square shaped avoidance region located adjacent to it. An L-shaped target with a region at risk located between the arms of the ''L'' was used to test a target of intermediate complexity. Finally, a U-shaped target has been used in the development of more complex treatment plans. This target has a rectangular region at risk located in the concavity of the U. Each of the three target shapes was cut out of a 5 cm by 5 cm square. The pencil beam data sets have also been used in simulations incorporating target shapes such as a torus and a pseudo-prostate. These results are presented elsewhere.[19,20]

After the pre-computed dose matrices are loaded into memory, the pencil beams are rotated to the specified angles. The weight of each beam is then optimized in order to produce the most favorable dose distribution. For the results presented in this paper, each optimization was performed using MATLAB's Optimization Toolbox.[21] A constrained nonlinear optimization routine called constr.m was used with all of the beam weights constrained to be nonnegative.[22] This optimization routine does not require the user to supply analytic gradients.

One useful implementation of these pencil beam data sets is as a tool for exploring the advantages and disadvantages a number of objective functions and optimization techniques. For example, the data sets have been used in a study of iterative approaches to dose optimization including the maximum likelihood estimator.[19,23] A variety of linear, nonlinear, and mixed integer approaches to dose optimization have also been tested using these pencil beams in conjunction with a number of commercial optimization software packages including CONOPT, MINOS, OSL, and CPLEX.[24–27] Approaches to dose reconstruction have also been tested using these data sets.[19]

This paper will not focus on optimization techniques. Instead, we will simply use a weighted least-squares objective function in all of the analysis.[11,13] In each simulation, the optimizer sought to minimize the sum over all pixels of a weighted squared difference between the prescribed and the actual dose. The only constraint that was applied was a nonnegativity constraint placed upon the beam weights. The optimizer sought to minimize the objective function shown below:

$$\text{Cost} = \Sigma_i TC_i + \Sigma_i NC_i ,$$

$$TC_i = (TW_i / N_T) * (D_i - D_{\text{pre}})^2 ,$$

$$NC_i = (NW_i / N_{\text{RAR}}) * (D_i)^2$$

where TC is the target cost, TW is the target weight, NC is the normal tissue cost, NW is the normal tissue weight, D_{pre} is the prescribed dose, D_i is the dose in voxel i, N_T is the number of tumor voxels, N_{RAR} is the number of voxels in RAR. Increasing the relative weight assigned to a target forces the optimizer to seek a more uniform dose over that target. By increasing the relative weight assigned to a normal tissue, one forces the optimizer to reduce the dose to that tissue.

TW_1 is the weight assigned to the target. NW_1 is the weight assigned to the sensitive structure, and NW_2 is the weight assigned to all other normal tissue. For our simulations, a single set of weighting factors was assigned previous to the optimization. It may be possible, however, to dynamically optimize the weighting factors, as was proposed by Hristov.[28]

The number of pixels in each region is used to normalize the weighting factor assigned to that region. This prevents a large sensitive structure from dominating the optimization.

Unless otherwise stated, the results presented in this paper used the following weights: $TW_1 = 15$, $NW_1 = 1$, $NW_2 = 1$. After a number of optimizations were performed, it was determined that these beam weights consistently produced quality dose distributions.

The least-squares objective function that was outlined above is a convex function. Thus the optimizer can provide the global minimum of the objective function. It is likely, however, that the solution will not be unique. In other words, there may be a number of beam weight combinations that produce the global minimum of the objective function. Thus the final dose distribution can in part depend upon the initial beam weight selection. Tests have been performed to explore the importance of this result.

C. Limitations

In any study making use of a model, it is essential that the user understand the limitations of the model. Some of the limitations of the pencil beam data sets are listed below:

(1) Only coplanar beams are available.
(2) Charged particle contamination ignored.
(3) Only photon beams are provided.
(4) Although the dose was computed in 3D, the optimizations are performed in a single slice.
(5) Two of the pencil beam data sets are parallel in nature.
(6) There are no heterogenieties with large atomic number differences.

This model does not provide the ability to include noncoplanar beams in the development of a treatment plan. Noncoplanar beams can be of assistance, particularly when a small number of beam angles are used. With a large number of beam angles, however, the benefit of adding noncoplanar beams is more limited.[18] In tomotherapy only coplanar beams are used.

The first two pencil data sets consist of monoenergetic parallel pencil beams with an energy of 2 MeV. Although the beams have a relatively low energy, the choice was considered appropriate for the 20-cm-diameter phantom.

It should also be noted that the dose computation did not account for charged particle contamination. Charged particle contamination is of particular importance with superficial targets where electron contamination can contribute substantially to the dose distribution.

III. RESULTS AND DISCUSSION

A. Beam delivery technique and target complexity

As an illustration of the potential benefits of IMRT, simulations have been run using three different delivery techniques. Through the summation of a series of adjacent pencil

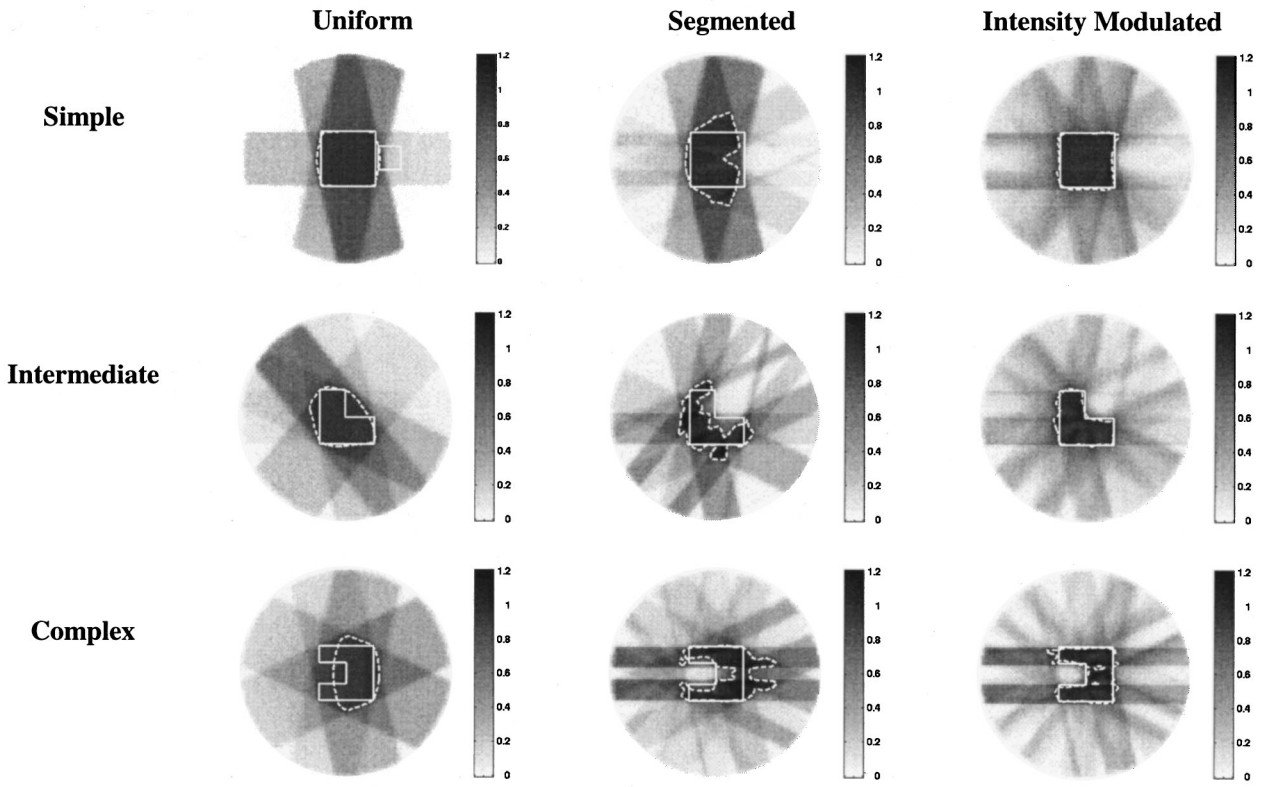

FIG. 3. The effectiveness of uniform, segmented, and intensity-modulated beam delivery is demonstrated for varying levels of target complexity. For all simulations, seven equispaced beam angles were used and the optimizer sought to provide a uniform target dose while minimizing the dose to the critical structure. Both uniform and segmented beam deliveries utilize open and unmodulated fields with the field size set to match the target dimensions. For segmented delivery, however, the portion of the field passing through the region at risk is blocked. The intensity modulated simulations utilized a collimator size of 6 mm, and each pencil beam was given a separate weight. The dashed line in each distribution denotes the 90% isodose curve with the mean dose defined as 100%.

TABLE I. Dependence upon collimator size using parallel pencil beams.

Collimator size (mm)	Standard deviation in dose over the target	Mean dose to region at risk
20	0.111	0.449
10	0.084	0.265
6	0.061	0.187
4	0.050	0.157
2	0.044	0.116

beams, one can produce uniform broad beams. This technique provides the opportunity to simulate the delivery of uniform or segmented fields for comparison with IMRT. Both uniform and segmented beam deliveries utilize open and unmodulated fields with the field size set to match the target dimensions. For segmented delivery, however, the portion of the field passing through the region at risk is blocked. The intensity-modulated simulations used a collimator size of 6 mm, and each pencil beam was given a separate weight.

Figure 3 compares optimized dose distributions obtained using all three delivery methods. In all cases, seven equispaced beam angles were used, and the beam weights were optimized using the weighted least-squares objective function. The benefits of intensity-modulation are most apparent with the complex target shape. Although segmented fields can provide a significant sparing of sensitive structures located in close proximity to the target, only IMRT can provide both sparing of the regions at a risk and dose uniformity in the target. In Fig. 3, one should note that IMRT provides the ability to provide tight contours matching the tumor shape.

B. Collimator size and few versus many angles

The collimator size and the number of beam angles both play important roles in determining one's ability to deliver a high quality treatment plan. In choosing a multi-leaf collimator, one must understand the relationship between the size of the collimators and the quality of the dose distributions that can be obtained. With our pre-computed pencil beams, one can bin together one or more adjacent beams in order to produce a new pencil beam of increased width. Thus a new effective collimator size is created.

Table I presents the results from a series of simulations using seven beam angles with a U-shaped target and a region at risk placed inside of the target's concavity (see Fig. 4). The objective function sought to deliver a relative dose of 1.0 to each pixel in the target while minimizing the dose to

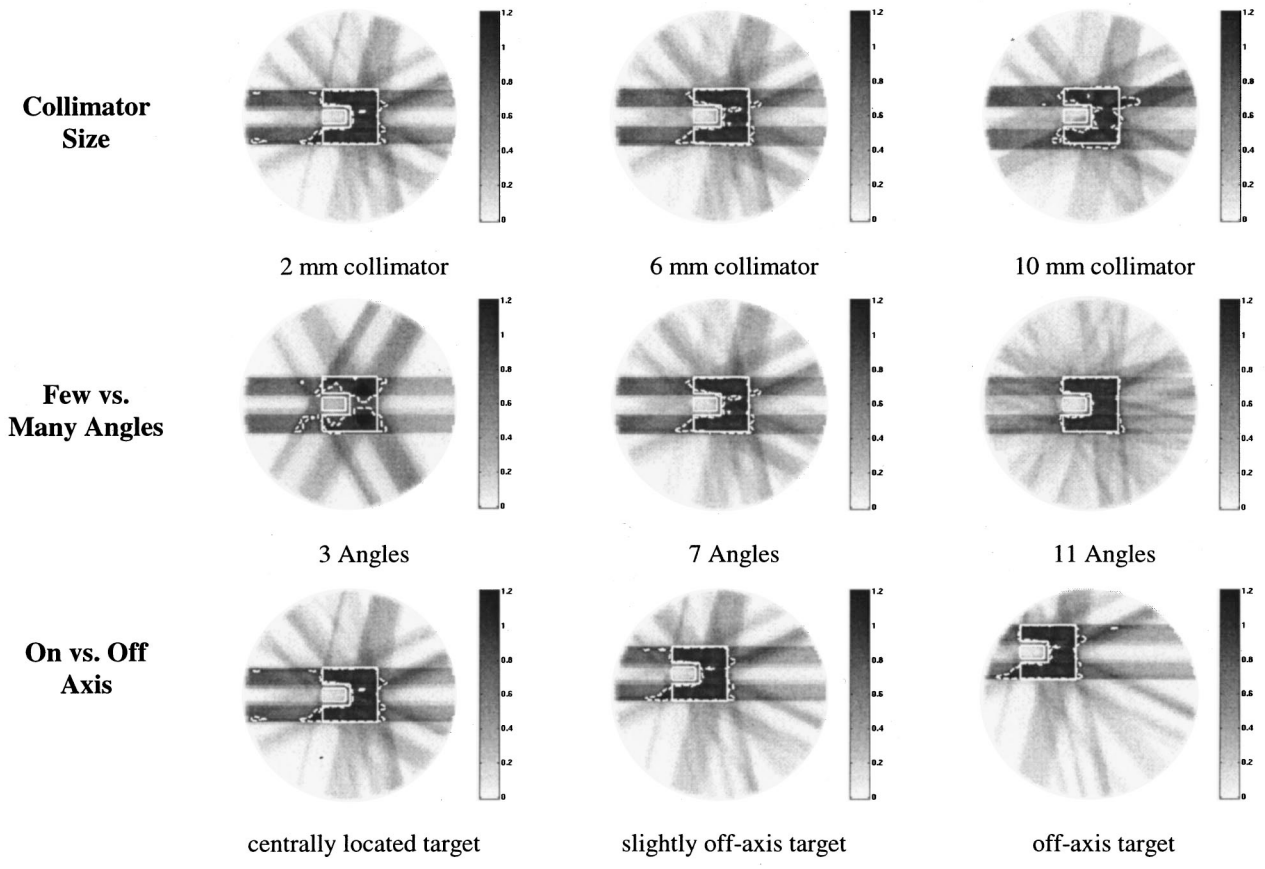

FIG. 4. The top row addresses the issue of collimator size. All of these simulations utilized seven equispaced angles, and only the collimator size was changed. The middle row of figures shows a series of dose distributions from simulations utilizing a 6-mm collimator setting. Only the number of angles was varied. For the bottom row of distributions, seven angles and a 4-mm collimator setting were used as only the target position was altered. The dashed line in each figure represents the 90% isodose curve with the mean dose defined as 100%.

TABLE II. Dependence upon collimator size using diverging pencil beams.

Collimator size (mm)	Standard deviation in dose over the target	Mean dose to region at risk
20	0.090	0.553
10	0.079	0.283
6	0.059	0.190
4	0.048	0.180
2	0.040	0.156

TABLE III. Dependence upon the number of angles.

Number of angles	Standard deviation in dose over target	Minimum target dose	Mean dose to RAR	Total integrated dose
3	0.124	0.644	0.488	2732.5
5	0.090	0.666	0.215	2563.3
7	0.064	0.797	0.206	2596.8
9	0.064	0.772	0.192	2598.3
11	0.058	0.775	0.186	2570.2
15	0.053	0.710	0.180	2542.9
21	0.049	0.768	0.171	2545.1
33	0.038	0.809	0.155	2543.5

the sensitive structure. Parallel pencil beams were used in this case. It can be seen that as the collimator size is progressively reduced from 2.0 cm to 0.2 cm, there is a marked improvement in the uniformity of the target dose.

The results shown in Table II were produced using the diverging pencil beams. A variety of collimator sizes were tested along with a U-shaped target and seven beam angles.

Comparing Tables I and II, one might note that the simulations that used parallel pencil beams always produced a more uniform target dose and a higher mean dose to the region at risk. One must be careful, however, in making this comparison, because the setup used in computing the diverging beams involved both a larger phantom and a different beam energy than was used in computing the parallel beams.

The use of an MLC with a small leaf size can be considered analogous to the use of a small detector size in imaging. A smaller leaf size provides an improved ability to deliver a dose distribution that incorporates high frequency components. Due to electron transport, however, the gains achievable with a decrease in the collimator size should reach a plateau. In Tables I and II, it is interesting to note that significant improvements in the dose distribution were obtained even as the leaf size was reduced to 2 mm. This is on the order of the distance of the lateral electron transport. Al-

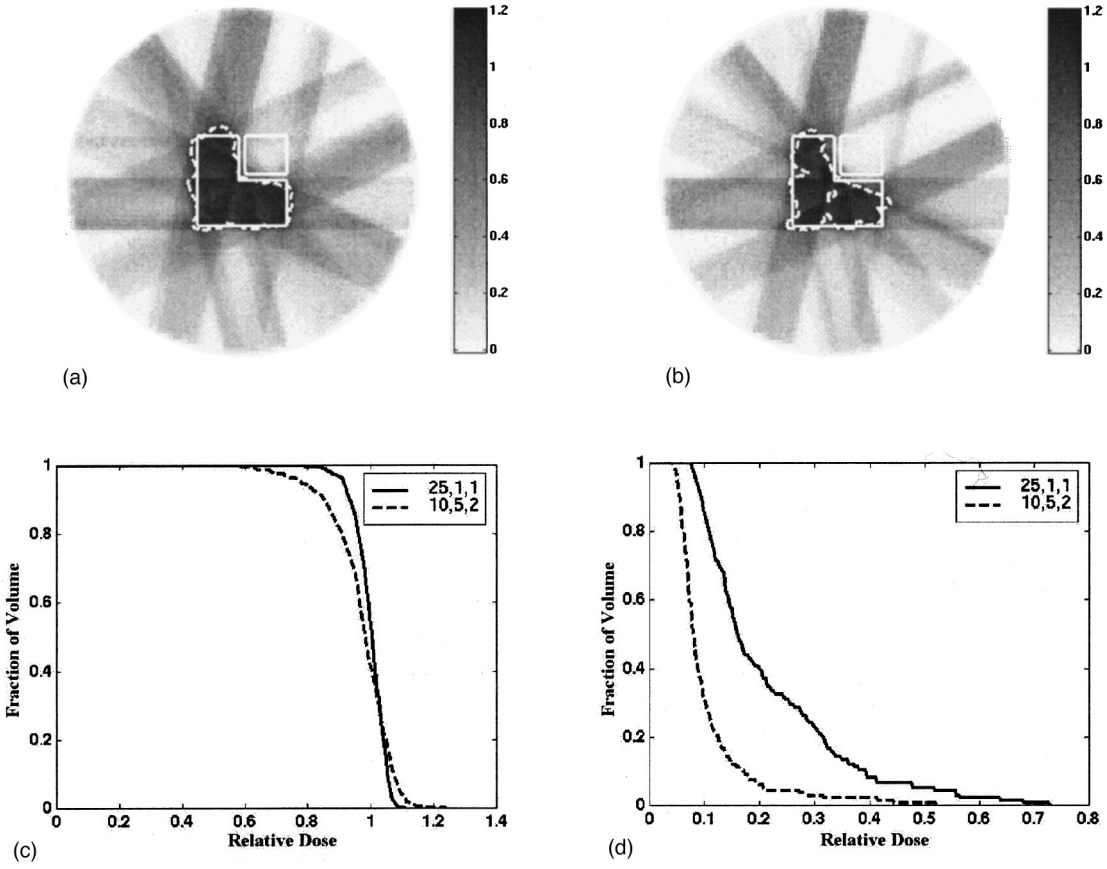

FIG. 5. The results from two simulations are shown. In both cases, a weighted quadratic objective function was used. For (a), the target, RAR, and normal tissue were assigned weights of 25, 1, and 1, respectively. In (b) the target, RAR, and normal tissues were assigned weights of 10, 5, and 2. In (c) the results are plotted for the target dose distributions, and (d) plots the results for the dose distributions in the region at risk. Note that the tumor dose is more uniform when the tumor was assigned a higher relative weight.

though the plateau was not reached, a leaf size smaller than 1 or 2 mm would be very difficult to implement from a technological point of view.

The optimal number of beam angles for the delivery of IMRT has been the subject of much debate.[3,29–31] For delivery methods other than tomotherapy, an increase in the number of angles can lead to a more complex and more time consuming treatment delivery. It is thus important to understand the correlation between the number of beam angles and the quality of the treatment plans that can be produced. A group of simulations have been run in which all parameters were held constant except for the number of beam angles. The simulations employed the U-shaped target. The collimator size was set at 0.6 cm, and the angles were equispaced. A few of the results are shown in Fig. 4, and more information is presented in Table III.

In Table III, the column of values showing the minimum target dose may appear somewhat perplexing. The minimum target dose seems to be independent of the number of beam angles. This inconsistency reveals a weakness of the simple quadratic objective function. The objective function is determined by summing squared differences over all of the voxels in the patient. Thus one individual voxel has very little influence on the total value of the objective function. As a result, a dose distribution that provides the optimal objective function value may significantly underdose a few target voxels in order to spare a neighboring sensitive structure. A suboptimal plan of this type could permit the survival of a small number of clonogens, and this could eventually lead to tumor recurrence.[32] One could attempt to prevent this underdosage by increasing the relative weight assigned to the target. This is illustrated in Fig. 5.

From Table III, it should also be noted that the mean dose to the region at risk changed by less than 2% as the number of beam angles was increased beyond seven. Of interest is the fact that the mean dose to the region at risk did not strictly decrease with each increase in the number of angles. One explanation of this result is that an increase in the mean dose to the region at risk can accompany a decrease in the objective function if there is a simultaneous improvement in the tumor dose uniformity. A second explanation is that, with equispaced beam angles, it is possible that an increase in the number of beam angles could lead to a slightly less optimal set of beam directions. For example, one can imagine that three equispaced beam angles might provide a more acceptable set of beam directions that two sets of parallel opposed beams. Thus the increase from three to four beam directions could actually degrade the quality of the treatment plan. With a large number of angles, however, this effect would not be seen.

TABLE IV. The addition of new beam angles to a pre-existing set of angles.

Number of angles	Standard deviation in dose over target	Minimum target dose	Mean dose to RAR	Total integrated dose
3	0.124	0.644	0.488	2732.5
6	0.111	0.689	0.336	2660.4
12	0.061	0.774	0.196	2484.2
24	0.045	0.794	0.170	2543.8

The preferred pencil beams are those that can irradiate the tumor while simultaneously sparing the sensitive structures. Initially, each increase in the number of beam angles provides a significant improvement in the available beam paths. For this particular setup, however, increasing the number of angles beyond nine had little effect on the target dose uniformity.

A second approach to the addition of beam angles has also been tested. After optimizing for an initial set of angles, new beams were added while maintaining the original beam positions. The new beams were placed between each of the existing beams. A new optimization was then performed. Results using this technique are shown in Table IV. When this approach to increasing the number of beams was used,

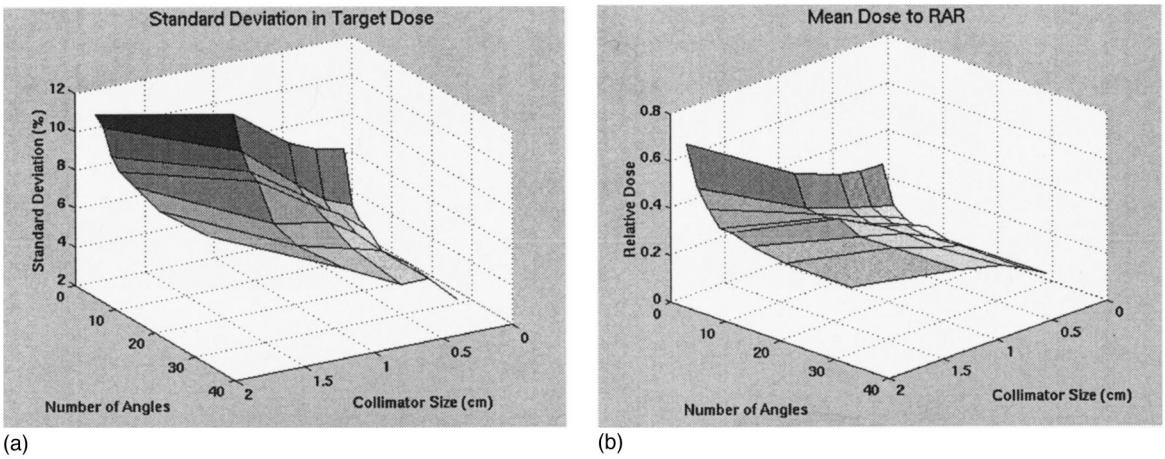

(a) (b)

FIG. 6. (a) This figure shows the results for the U-shaped target. Note that a more uniform target dose is obtained as the number of angles increases and the collimator size decreases. (b) For the RAR located in the concavity of the U, the mean dose is reduced as the number of angles is increased and the collimator size is reduced.

TABLE V. Percent standard deviation in the target dose as a function of the collimator size and the number of beam angles for the U-shaped target.

		Collimator size (cm)				
		2.0	1.0	0.6	0.4	0.2
Number of angles	3	10.5	12.1	11.8	11.7	11.6
	5	11.5	10.1	8.0	7.4	7.1
	7	11.1	8.4	6.1	5.0	4.4
	9	9.8	7.6	5.7	4.5	3.8
	11	9.3	7.3	5.5	4.7	3.6
	15	9.0	5.6	5.1	4.2	2.9
	21	8.5	5.2	4.5	4.1	3.1
	33	8.7	5.5	4.1	4.1	2.7

each parameter improved continuously as the number of beam angles was increased.

From the last column in Tables III and IV, it is important to note that the total integrated dose is nearly independent of the number of angles. Changing the number of angles simply alters the manner in which the same integral dose is ''spent.'' Thus a rotational beam delivery such as tomotherapy should not increase the integral dose or the total energy delivered to the patient.

The combined effects of changes in the collimator size and the number of beam angles for the U-shaped target are shown in Fig. 6. The results are also presented in Table V and Table VI. In general, as the number of angles is increased and the collimator size is decreased, one will see both a lower standard deviation in dose over the target and a lower mean dose to the region at risk. This is analogous to computed tomography (CT) where the image quality improves as the number of projections is increased and the detector size is decreased.

In each optimization, a compromise is reached between the need for target uniformity and the desire to spare the sensitive structure. With a small number of beam angles and a large collimator size, these two goals can become mutually exclusive. This can be seen in Fig. 6 when three beam angles were used along with a collimator size of 2 cm. For those settings, the final dose distribution provided a uniform target dose with very little sparing of the sensitive structure.

TABLE VI. Mean dose to the region at risk as a function of the collimator size and the number of beam angles for the U-shaped target.

		Collimator size (cm)				
		2.0	1.0	0.6	0.4	0.2
Number of angles	3	0.696	0.406	0.335	0.315	0.310
	5	0.526	0.275	0.209	0.182	0.153
	7	0.449	0.265	0.187	0.157	0.116
	9	0.386	0.266	0.174	0.141	0.098
	11	0.385	0.278	0.180	0.156	0.114
	15	0.357	0.232	0.182	0.134	0.087
	21	0.337	0.235	0.172	0.148	0.089
	33	0.329	0.239	0.191	0.145	0.092

TABLE VII. Dependence upon target location—centrally located.

	Minimum dose	Maximum dose	Mean dose	Sum
Target	0.77	1.13	0.99	539.0
Region at risk	0.14	0.50	0.23	15.0
Non-PTV	0.00	1.05	0.30	2264.3
Total dose				2803.3

C. Target location

Simulations have been run using a number of different target locations. The goal of these simulations was to examine the extent to which target location influences the ability to achieve a uniform target dose distribution.

Two simulations were run at different off-axis locations using seven beam angles, a collimator size of 6 mm, and the U-shaped target. In Table VII, the results are shown for a centrally located target. In Table VIII, the results are tabulated from a simulation using a target located in the periphery of the cylinder. This off-axis target was located far enough from the surface of the phantom so that the neglect of charged particle contamination should not have had a significant impact on the results. In both cases, the tumor was prescribed a dose of one and a dose of zero was prescribed elsewhere.

In the Tables VII and VIII, the ''non-PTV'' region incorporated all of the pixels located outside both the target and the region at risk. The total integrated dose was approximately 17% higher for the centrally located target. The peripheral target location results in a reduction in the integral dose, because greater emphasis can be placed upon those beams that enter the patient in close proximity to the tumor. The results from a number of simulations suggest that the placement of the target does not significantly impact the ability to achieve a uniform target dose and spare the sensitive structure (see Fig. 4).

D. Inhomogeneities

The second simulated phantom has provided an opportunity to study the extent to which inhomogeneities perturb the dose distribution. A set of simulations was run using the water-and-lung phantom. Next, the beams computed for the all-water phantom were used in a new set of simulations that incorporated the same target setups. For comparison, the beam weights from the all-water simulations were applied to the water-and-lung phantom. For example, Table IX shows results obtained from an optimization using the water-and-

TABLE VIII. Dependence upon target location—peripherally located.

	Minimum dose	Maximum dose	Mean dose	Sum
Target	0.72	1.17	0.99	540.4
Region at risk	0.08	0.44	0.17	11.1
Non PTV	0.00	1.06	0.23	1790.2
Total dose				2330.6

TABLE IX. Results of optimization performed on the water-and-lung phantom using inhomogeneity corrected pencil beams.

	Minimum dose	Maximum dose	Mean dose	Sum
Target	0.76	1.10	0.99	539.7
Region at risk	0.13	0.53	0.25	16.8

TABLE X. Results of applying all-water optimized beam weights to water-and-lung phantom.

	Minimum dose	Maximum dose	Mean dose	Sum
Target	0.76	1.16	1.02	558.6
Region at risk	0.19	0.57	0.30	19.6

lung phantom with nine angles and a 6-mm collimator setting. An off-axis U-shaped target was used with the target straddling both the lung and the water portions of the phantom. Next, a second optimization was run using the same setup and the all-water phantom. The beam weights calculated for the all-water phantom were then applied to the beams computed for the water-and-lung phantom. The results are shown in Table X.

The maximum dose to the target and region at risk were both increased, but the cumulative dose volume histogram was relatively unaffected. The relative change in the dose distribution was influenced by two distinct phenomena. First, the beams passing through the lung region were attenuated less rapidly than were those that only passed through water. Second, the portion of the tumor located in the lung had a lower attenuation coefficient. A greater fluence was thus needed to deposit the required dose to the lower density region. The dose distributions for the two simulations along with their corresponding cumulative dose volume histograms are shown in Fig. 7.

For this case, a failure to properly correct for the phantom's inhomogeneity primarily affected the absolute rather than the relative dose distribution. In order to further our understanding of the importance of heterogeneity corrections, we ran simulations with a variety of initial beam angles. In all instances, the beam weights for the all-water case followed a pattern similar to that for the water-and-lung case. It should be noted, however, that with a high density inhomogeneity, there would be a much greater impact on the contours of the dose distribution.

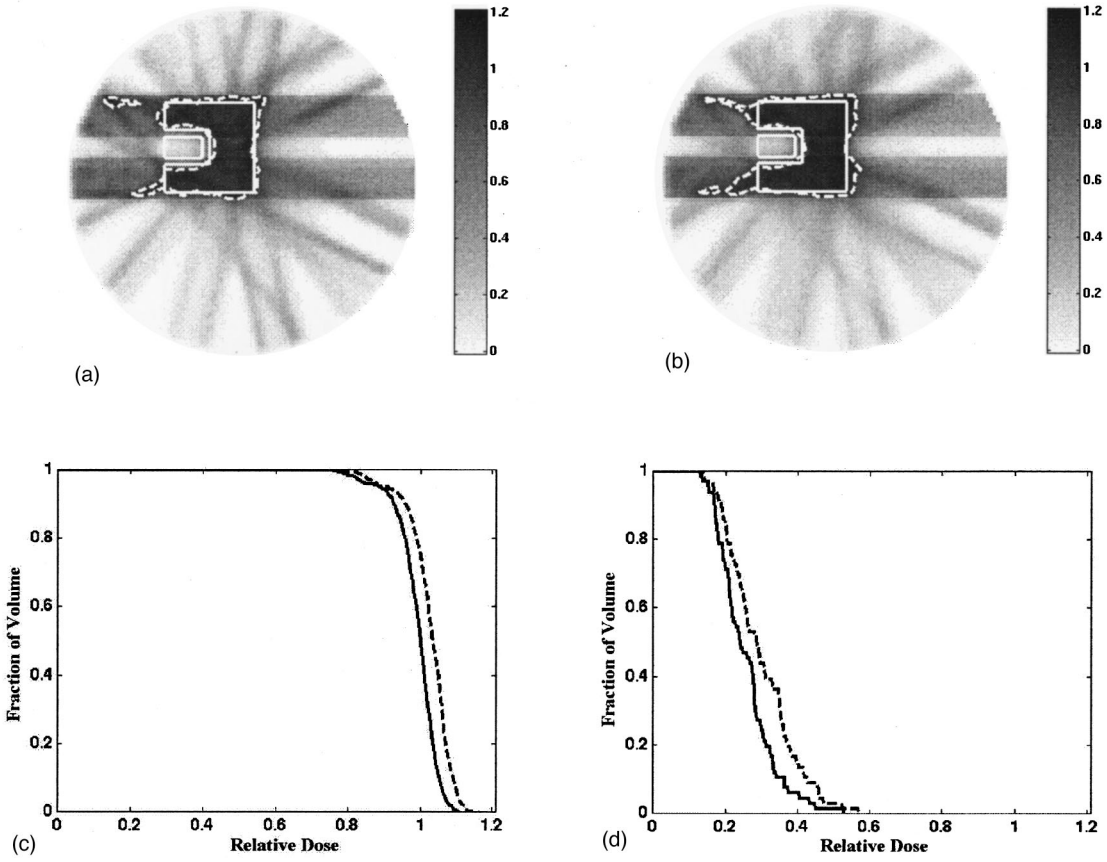

FIG. 7. (a) The optimized dose distribution for the U-shaped target with proper heterogeneity corrections. The lower left portion of the target is located within the centrally located lung heterogeneity. The dashed line represents the 90% isodose line. (b) Optimized beam weights were computed for the all-water phantom. Those beam weights were then applied to the properly heterogeneity corrected pencil beams. Note the change in the 90% isodose line. (c) and (d) The cumulative dose volume histograms for the target and region at risk respectively. In (c) and (d), the solid line plots the result from (a) and the dashed line plots the result from (b).

Our results suggest that it may be useful to optimize a treatment plan without heterogeneity corrections. This would permit the use of a very simple dose engine that could provide a significant speed up. The resultant beam weights could then be used as an initial guess in an optimization that includes an accurate heterogeneity correction. Overall, this technique might provide a more rapid path to an acceptable solution.

IV. CONCLUSIONS

A simple model for investigating issues in IMRT has been presented. The pencil beam data sets have been designed to serve as a tool for education and investigation in radiotherapy. Their usefulness has been demonstrated through a number of studies. The pencil beam data sets along with the code used to compute them have been made publicly available through our website at www.madrad.radiology.wisc.edu. We are currently using these pencil beams in an extensive study into the advantages and disadvantages of a number of optimization approaches.

[a]Present address: Department of Radiation Oncology, University of Maryland School of Medicine, Baltimore, MD 21201-1532.

[1]T. Bortfeld, A. L. Boyer, W. Schlegel, D. L. Kahler, and T. J. Waldron, ''Realization and verification of three-dimensional conformal radiotherapy with modulated fields [see comments],'' Int. J. Radiat. Oncol., Biol., Phys. **30**, 899–908 (1994).

[2]A. L. Boyer, ''Present and future developments in radiotherapy treatment units,'' Seminars in Radiation Oncology **5**, 146–155 (1995).

[3]A. Brahme, ''Optimization of radiation therapy and the development of multileaf collimation,'' Int. J. Radiat. Oncol., Biol., Phys. **25**, 373–375 (1993).

[4]M. Carol, H. Targovnik, D. Smith, and D. Cahill, ''3-D planning and delivery system for optimzed conformal therapy,'' Int. J. Radiat. Oncol., Biol., Phys. **24**, 159 (1992).

[5]M. Carol, W. H. Grant, A. R. Bleier, A. A. Kania, H. Targovnik, E. B. Butler, and S. W. Woo, ''The field-matching problem as it applies to the Peacock three dimensional conformal system for intensity modulation,'' Int. J. Radiat. Oncol., Biol., Phys. **34**, 183–187 (1996).

[6]O. Dahl, D. Kardamakis, B. Lind, and J. C. Rosenwald, ''Current status of conformal radiotherapy,'' Acta Oncol. **35**, 41–57 (1996).

[7]Z. Fuks, S. Leibel, G. J. Kutcher, R. Mohan, and C. C. Ling, ''Three-dimensional conformal treatment: A new frontier in radiation therapy,'' Important Advances in Oncology, 151–172 (1991).

[8]D. D. Leavitt, M. Martin, J. H. Moeller, and W. Lok Lee, ''Dynamic wedge field techniques through computer-controlled collimator motion and dose delivery,'' Med. Phys. **17**, 87–92 (1990).

[9]T. R. Mackie, T. Holmes, S. Swerdloff, P. Reckwerdt, J. O. Deasy, J. Yang, B. Paliwal, and T. Kinsella, ''Tomotherapy: A new concept for the delivery of dynamic conformal radiotherapy,'' Med. Phys. **20**, 1709–1719 (1993).

[10]R. Mohan, ''Field shaping for three-dimensional conformal radiation therapy and multileaf collimation,'' Seminars in Radiation Oncology **5**, 86–99 (1995).

[11]E. S. Sternick, *The Theory and Practice of Intensity Modulated Radiation Therapy* (Advanced Medical Publishing, Madison, WI, 1997).

[12]L. J. Verhey, ''3-D conformal therapy using beam intesity modulation,'' Frontiers in Radiation Therapy and Oncology **29**, 139–155 (1996).

[13]S. Webb, *The Physics of Conformal Radiotherapy: Advances in Technology* (IOP Publishing, Philadelphia, 1997).

[14]T. R. Mackie, J. W. Scrimger, and J. J. Batista, ''A convolution method of calculating dose from 15 MeV x-rays,'' Med. Phys. **12**, 188–196 (1985).

[15]N. Papanikolaou, T. R. Mackie, C. Meger-Wells, M. Gehring, and P. Reckwerdt, ''Investigation of the convolution method for polyenergetic spectra,'' Med. Phys. **20**, 1327–1336 (1993).

[16]T. R. Mackie, P. Reckwerdt, and N. Papanikolau, ''3-D photon beam dose algorithms,'' presented at the 3-D Radiation Treatment Planning and Conformal Therapy, St. Louis, MO, 1993 (unpublished).

[17]D. M. Shepard, L. Angelos, O. A. Sauer, and T. R. Mackie, ''A simple model for examining radiotherapy optimization,'' presented at the XII International Conference on the Use of Computers in Radiation Therapy, Salt Lake City, Utah, 1997 (unpublished).

[18]M. Oldham, V. S. Khoo, C. G. Rowbottom, J. L. Bedford, and S. Webb, ''A case study comparing the relative benefit of optimizing beam weights, wedge angles, beam orientations and tomotherapy in stereotactic radiotherapy of the brain,'' Phys. Med. Biol. **43**, 2123–2146 (1998).

[19]G. H. Olivera, D. Shepard, P. J. Reckwerd, K. Ruchala, J. Zachman, E. E. Fitchard, and T. R. Mackie, ''Maximum likelihood as a common computational framework in tomotherapy,'' Phys. Med. Biol. **43**, 3277–3294 (1998).

[20]D. M. Shepard, G. H. Olivera, P. J. Reckwerdt, and T. R. Mackie, ''Iterative approaches to dose optimization in tomotherapy,'' Phys. Med. Biol. (submitted).

[21]A. Grace, *Optimization Toolbox for Use with Matlab* (The Mathworks, Inc., Natick, MA, 1995).

[22]P. E. Gill, W. Murray and M. H. Wright, *Practical Optimization* (Academic, London, 1981).

[23]J. Llacer, ''Bayesian smoothing for iterative inverse radiation treatment planning,'' presented at the American Association of Physicists in Medicine, San Antonio, 1998 (unpublished).

[24]D. M. Shepard, M. C. Ferris, G. H. Olivera, and T. R. Mackie, ''Optimizing the delivery of radiation therapy to cancer patients,'' SIAM (Soc. Ind. Appl. Math.) Rev. (accepted) (1998).

[25]*Using the CPLEX(TM) Linear Optimizer and CPLEX(TM) Mixed Integer Optimization (Version 2.0)* (CPLEX Optimization Inc., Incline Village, Nevada, 1992).

[26]A. Drud, ''CONOPT: A GRG code for large sparse dynamic nonlinear optimization problems,'' Math. Program. **31**, 153–191 (1985).

[27]B. A. Murtagh and M. A. Saunders, *MINOS 5.0 user's guide* (Stanford University, Stanford, CA, 1983).

[28]D. H. Hristov and B. G. Fallone, ''A continuous penalty function method for inverse treatment planning,'' Med. Phys. **25**, 208–223 (1998).

[29]R. Mohan and C. Ling, ''When becometh less more,'' Int. J. Radiat. Oncol., Biol., Phys. **33**, 235–237 (1995).

[30]S. Soderstrom and A. Brahme, ''Which is the most suitable number of photon beam portals in coplanar radiation therapy? [see comments],'' Int. J. Radiat. Oncol., Biol., Phys. **33**, 151–159 (1995).

[31]T. R. Mackie, J. Deasy, T. Holmes, and J. Fowler, ''Letter in response to 'Optimization of radiation therapy and the development of multileaf collimation' by Anders Brahme,'' Int. J. Radiat. Oncol., Biol., Phys. **28**, 784–785 (1994).

[32]S. Leibel and Z. Fuks, ''The impact of local tumor control on the outcome in human cancer,'' presented at the 3-D Radiation Treatment Planning and Conformal Therapy, St. Louis, MO, 1993 (unpublished).